Experimental confirmation at visible light wavelengths of the backscattering enhancement phenomenon of the photonic nanojet

Seungmoo Yang,[1,*] Allen Taflove,[2] and Vadim Backman[1]

[1]*Department of Biomedical Engineering, Northwestern University, McCormick School of Engineering, 2145 Sheridan Road, Evanston, Illinois 60208, USA*
[2]*Department of Electrical Engineering and Computer Science, Northwestern University, McCormick School of Engineering, 2145 Sheridan Road, Evanston, Illinois 60208, USA*
**seungmoo-yang@northwestern.edu*

Abstract: We report what we believe is the first experimental confirmation at visible light wavelengths of the backscattering enhancement phenomenon of the photonic nanojet. A specially designed sample stage consisting of a multilayered sandwich of glass, solid polydimethylsiloxane (PDMS), and liquid PDMS, permitted the precise positioning of a gold nanoparticle of diameter between 50 and 100 nm within the nanojet emitted by a 4.4 μm diameter $BaTiO_3$ microsphere embedded within the PDMS. We determined that, when the gold nanoparticle is optimally positioned within the nanojet, the backscattering of the microsphere can greatly increase: for example, by 3:1 (200%) for the 50 nm gold nanoparticle. The increased backscattering is strongly dependent upon the illumination wavelength and the numerical aperture of the imaging system, and occurs for nonresonant illuminations of the isolated microsphere. Low objective numerical apertures of approximately 0.075 yield the maximum observed increases in backscattering. The measured data agree well with numerical calculations incorporating Mie-based theory and Fourier optics.

OCIS codes: (170.0170) Medical optics and biotechnology; (290.5850) Scattering, particles; (290.1350) Backscattering.

References and links

1. Z. Chen, A. Taflove, and V. Backman, "Photonic nanojet enhancement of backscattering of light by nanoparticles: a potential novel visible-light ultramicroscopy technique," Opt. Express **12**(7), 1214–1220 (2004).
2. P. Ferrand, J. Wenger, A. Devilez, M. Pianta, B. Stout, N. Bonod, E. Popov, and H. Rigneault, "Direct imaging of photonic nanojets," Opt. Express **16**(10), 6930–6940 (2008).
3. S. Lecler, Y. Takakura, and P. Meyrueis, "Properties of a three-dimensional photonic jet," Opt. Lett. **30**(19), 2641–2643 (2005).
4. A. V. Itagi and W. A. Challener, "Optics of photonic nanojets," J. Opt. Soc. Am. A **22**(12), 2847–2858 (2005).
5. A. Devilez, B. Stout, N. Bonod, and E. Popov, "Spectral analysis of three-dimensional photonic jets," Opt. Express **16**(18), 14200–14212 (2008).
6. A. Devilez, B. Stout, and N. Bonod, "Compact metallo-dielectric optical antenna for ultra directional and enhanced radiative emission," ACS Nano **4**(6), 3390–3396 (2010).
7. Z. Wang, W. Guo, L. Li, B. Luk'yanchuk, A. Khan, Z. Liu, Z. Chen, and M. Hong, "Optical virtual imaging at 50 nm lateral resolution with a white-light nanoscope," Nat. Commun. **2**, 218 (2011), doi:10.1038/ncomms1211.
8. X. Li, Z. Chen, A. Taflove, and V. Backman, "Optical analysis of nanoparticles via enhanced backscattering facilitated by 3-D photonic nanojets," Opt. Express **13**(2), 526–533 (2005).
9. Z. Chen, A. Taflove, X. Li, and V. Backman, "Superenhanced backscattering of light by nanoparticles," Opt. Lett. **31**(2), 196–198 (2006).
10. A. Heifetz, K. Huang, A. V. Sahakian, X. Li, A. Taflove, and V. Backman, "Experimental confirmation of backscattering enhancement induced by a photonic jet," Appl. Phys. Lett. **89**(22), 221118 (2006).
11. L. Zhao and C. K. Ong, "Direct observation of photonic jets and corresponding backscattering enhancement at microwave frequencies," J. Appl. Phys. **105**(12), 123512 (2009).

#142019 - $15.00 USD Received 31 Jan 2011; revised 21 Mar 2011; accepted 21 Mar 2011; published 29 Mar 2011

12. S.-C. Kong, A. V. Sahakian, A. Heifetz, A. Taflove, and V. Backman, "Robust detection of deeply subwavelength pits in simulated optical data-storage disks using photonic jets," Appl. Phys. Lett. **92**(21), 211102 (2008).
13. S.-C. Kong, A. Sahakian, A. Taflove, and V. Backman, "Photonic nanojet-enabled optical data storage," Opt. Express **16**(18), 13713–13719 (2008).
14. P. B. Johnson and R. W. Christy, "Optical constants of the noble metals," Phys. Rev. B **6**(12), 4370–4379 (1972).
15. Y. L. Xu, "Electromagnetic scattering by an aggregate of spheres," Appl. Opt. **34**(21), 4573–4588 (1995).
16. Y. L. Xu, "Scattering Mueller matrix of an ensemble of variously shaped small particles," J. Opt. Soc. Am. A **20**(11), 2093–2105 (2003).

1. Introduction

The photonic nanojet is a purely linear phenomenon wherein an illuminated dielectric microparticle emits from its shadow-side surface a tightly focused beam which propagates with little divergence for several wavelengths in the external medium [1–3]. Detailed analyses of the physics basis of the photonic nanojet, which are beyond the scope of the present paper, are provided in [4,5]. Recently, interest in the related optical properties of dielectric microspheres has prompted important papers reporting advances in ultra-directional optical antennas [6] and subdiffraction-resolution optical virtual imaging [7].

One of the most interesting properties of the photonic nanojet is that the backscattering of the dielectric particle from which it emerges can be greatly increased by the passage of a much smaller metal particle through the nanojet [1,8–11]. In these papers, numerical models and dimensionally scaled microwave experiments have shown that, when translated along the axis of the nanojet, a tiny metal particle only 1/100th the diameter of the dielectric particle (i.e., only 1/10,000th its physical cross-section) can approximately double the backscattered power of the dielectric particle. However, to the best of our knowledge, there has not yet been a direct experimental verification and measurement of this phenomenon at any visible light wavelength. Such verification and measurement is required to help realize proposed technology applications in nanoparticle detection/sizing and ultrahigh-density optical data storage [12,13].

To this end, we report in this paper what we believe is the first experimental confirmation at visible light wavelengths of the backscattering enhancement phenomenon of the photonic nanojet. For a dielectric microsphere a few microns in diameter, the backscattering enhancement is found to be strongly dependent upon the optical wavelength and the numerical aperture of the imaging system. The measured data agree well with numerical calculations incorporating Mie-based theory and Fourier optics.

2. Optical imaging experiment sample platform

Repeatable experimental measurements at visible light wavelengths of the backscattering enhancement phenomenon of the photonic nanojet requires precisely positioning in three dimensions a metal nanoparticle (diameter ~50 – 100 nm) at the peak intensity point of the narrow (< 500 nm waist) photonic nanojet which extends outward several microns from the shadow-side surface of a dielectric microsphere (diameter ~5 μm) along its front-back axis. All this must occur while minimizing optical reflections caused by the positioning apparatus.

To facilitate these experimental requirements, we employed polydimethylsiloxane (PDMS) of refractive index $n = 1.41$ as the background medium in which both the dielectric microsphere and gold nanoparticles were embedded. This required using a high-index $BaTiO_3$ microsphere ($n_\mu = 2.1$) having an appropriate refractive index contrast to the background medium to enable generation of a nominal nanojet configuration (length, waist) over the desired illumination wavelength range, 400 nm < λ_0 < 700 nm. Each gold nanoparticle used had an index at $\lambda_0 = 400$ nm of $1.47 - j1.95$ [14].

#142019 - $15.00 USD Received 31 Jan 2011; revised 21 Mar 2011; accepted 21 Mar 2011; published 29 Mar 2011

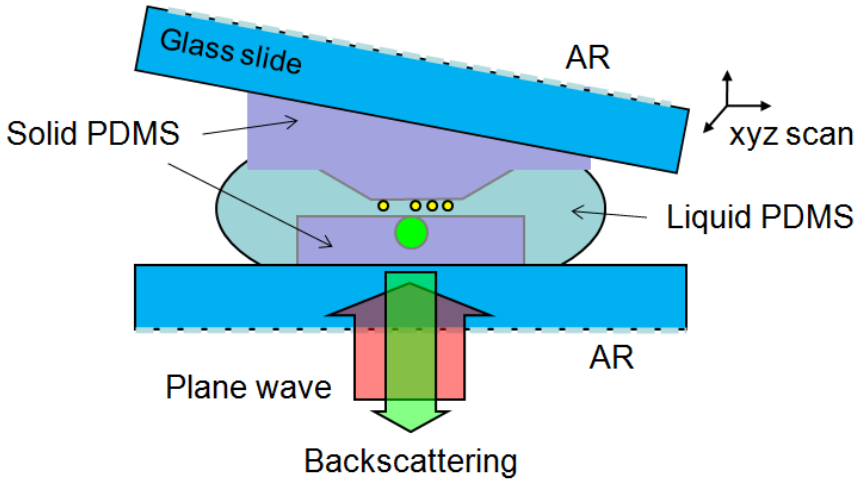

Fig. 1. Schematic diagram of the $BaTiO_3$ microsphere – gold nanoparticle sample platform.

Figure 1 is a schematic diagram of the sandwich-type microsphere – nanoparticle sample platform. The outer layers of the sandwich were comprised of a pair of glass slides, with each slide having a single antireflection (< 0.5%) coated surface facing outward to the air. The top glass slide was tilted to further reduce direct backscattering reflections from its surfaces. Inward from, and immediately adjacent to each glass slide was a solid PDMS layer. Optical reflection at the interface of each glass slide and its adjacent solid PDMS layer was found to be only about 0.1%. The $BaTiO_3$ microsphere was embedded in the lower solid PDMS layer with the microsphere touching the top surface of this layer. (This embedding was very stable after curing for 2 hours at 100°C.) At the center of the sandwich between the two solid PDMS layers, a central region of liquid PDMS contained a suspension of gold nanoparticles. These attached randomly to the bottom surface of the upper solid PDMS layer.

The microsphere – nanoparticle platform of Fig. 1 was mounted on the sample stage of a conventional inverted microscope, the Leica DMIRB. Two independent observation configurations, the imaging mode and the detection mode, were employed. The imaging mode involved a conventional reflection microscope setup to image and monitor the location of a nanoparticle relative to the microsphere. Here, a high-magnification (40X) objective was used with a large numerical aperture (NA = 0.65) illuminated by a halogen source. In the detection mode, a mercury arc lamp illuminated the sample platform from the bottom with a quasi-plane wave through a low NA objective (5X, NA = 0.12). The backscattered intensity was collected with the same objective and fed to the imaging spectrometer which recorded the spectra and images of the microsphere – nanoparticle combination.

With the sandwich structure of Fig. 1, the relative position of the two solid PDMS layers could be adjusted in three dimensions because the liquid PDMS (which did not have a curing agent) lubricated both contact surfaces. Using a three-axis hydraulic micromanipulator, the top solid PDMS layer was positioned to move one of the gold nanoparticles bound to its bottom surface toward the center axis of the microsphere located in the solid PDMS layer below. This positioning was monitored using the high-magnification imaging mode. Once the gold nanoparticle was positioned close to the center axis of the microsphere, the imaging mode was switched to the detection mode. Then, the backscattered intensity and spectrum was recorded as the nanoparticle was translated through the nanojet by further careful tuning of the micromanipulator.

#142019 - $15.00 USD Received 31 Jan 2011; revised 21 Mar 2011; accepted 21 Mar 2011; published 29 Mar 2011

3. Theoretical backscattering spectrum—ideal plane-wave illumination

We first report a theoretical study of the wavelength dependence of the backscattering enhancement phenomenon for a simplified, idealized version of the experiment described in Section 2 above. In this idealization, the backscattering of a plane-wave-illuminated 4.4 μm $BaTiO_3$ microsphere (n_μ = 2.1) embedded within an infinite PDMS space (n = 1.41) is calculated for two cases: (1) the isolated microsphere, and (2) the microsphere with a 60 nm spherical gold nanoparticle optimally located within the nanojet generated by the plane-wave illumination of the microsphere. The complex-valued wavelength-dependent refractive index of gold is taken from [14]. We define the normalized incremental backscattering intensity enhancement δI associated with this system as reported in [8]:

$$\delta I \equiv \frac{\Delta I}{I_\mu} = \frac{I_{\mu+\nu} - I_\mu}{I_\mu} \tag{1}$$

where I_μ is the backscattered intensity of the isolated $BaTiO_3$ microsphere, and $I_{\mu+\nu}$ is the backscattered intensity of the $BaTiO_3$ microsphere / gold nanoparticle system. Effectively, δI is in units of I_μ. The range $0 < \delta I < 1$ represents minor (but possibly still detectable) backscattering enhancements, whereas the range $\delta I > 1$ represents major backscattering enhancements. This factor was calculated as a function of wavelength using a validated generalized multisphere Mie (GMM) code [15].

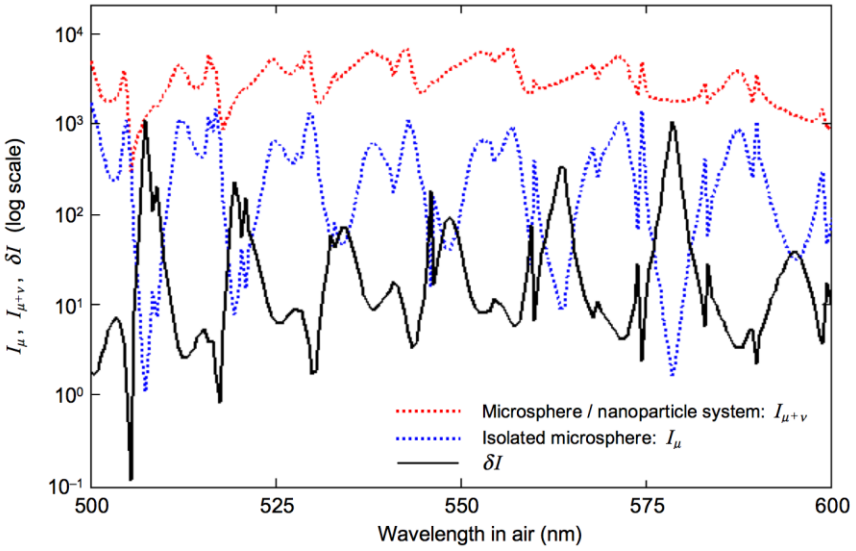

Fig. 2. Normalized incremental backscattering intensity enhancement δI vs. wavelength for the idealized $BaTiO_3$ microsphere / gold nanoparticle system.

Figure 2 shows the results of this study. The backscattering intensity I_μ for the isolated microsphere is plotted as the blue dotted curve, and the backscattering intensity $I_{\mu+\nu}$ for the composite microsphere/nanoparticle system is plotted as the red dotted curve. The continuous black curve plots the normalized incremental backscattering intensity enhancement δI. We observe that δI is strongly wavelength-dependent. Relatively large values of δI occur at wavelengths where the isolated microsphere exhibits no resonances and its backscattering intensity is small.

#142019 - $15.00 USD Received 31 Jan 2011; revised 21 Mar 2011; accepted 21 Mar 2011; published 29 Mar 2011

4. Backscattering enhancement simulation tool

In most practical applications using visible light, optical imaging systems are necessary since the scales of the operating wavelength and the samples of interest are much smaller than the scale of the geometry of the detection system. We expect the backscattering intensity enhancement observed using a practical imaging system to differ from the ideal plane-wave assumptions of Section 3 since an imaging system sums incoherently any wavelength dependencies, such as shown in Fig. 2. Furthermore, an optical imaging system employs a nonzero numerical aperture (NA) which sums coherently over the scattering angle.

In order to compare our experimental results with an appropriate theoretical calculation, a numerical simulation tool incorporating Fourier optics and the rigorous GMM solution of Maxwell's equations was developed. Figure 3 depicts the assumed imaging geometry.

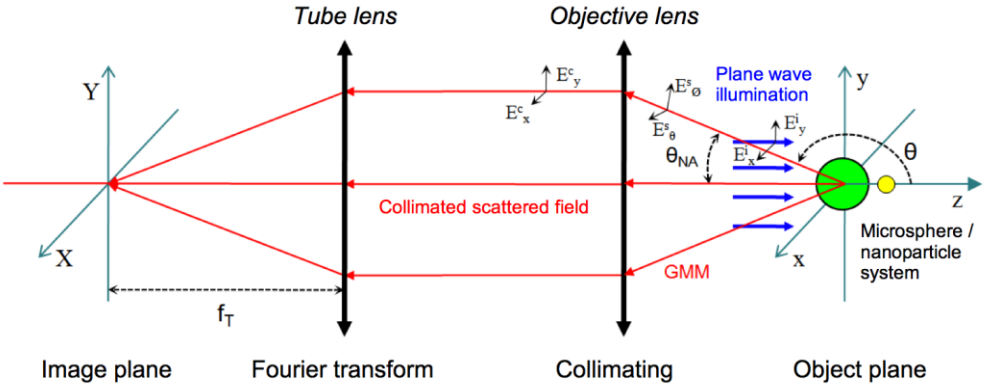

Fig. 3. Optical imaging detection scheme which performs a Fourier transformation of the collimated scattered fields from the microsphere / nanoparticle system.

Referring to Fig. 3, a linearly polarized, monochromatic plane wave propagating in the +*z*-direction with the incident field components, E_x^i and E_y^i, is assumed to illuminate the microsphere/nanoparticle system wherein the microsphere is centered in the object plane. In the far field, the scattered field components, E_θ^s and E_ϕ^s, in spherical coordinates are calculated from the GMM theory. These field components are related to the incident field components by the 2 × 2 amplitude matrix **S** [15,16]:

$$\begin{pmatrix} E_\theta^s \\ E_\phi^s \end{pmatrix} = \frac{e^{ikr}}{ikr} \mathbf{S} \begin{bmatrix} \cos\phi & \sin\phi \\ -\sin\phi & \cos\phi \end{bmatrix} \begin{pmatrix} E_x^i \\ E_y^i \end{pmatrix} \tag{2}$$

where *k* is the wavenumber of the incident field in the surrounding medium.

An objective lens is assumed to collect (i.e., integrate) these scattered fields over the complete azimuthal angle range $0 < \phi < 360°$ about the –*z*-axis, and over the zenith angle range $180° - \theta_{NA} < \theta < 180°$ with respect to the + *z*-axis. This collection cone is determined by the NA of the objective lens. Then, the objective lens is assumed to convert the diverging scattered fields in spherical coordinates into collimated fields in Cartesian coordinates, wherein the collimated field components, E_x^c and E_y^c, are obtained by:

$$\begin{pmatrix} E_x^c \\ E_y^c \end{pmatrix} = \begin{bmatrix} \cos\phi & \sin\phi \\ -\sin\phi & \cos\phi \end{bmatrix} \begin{pmatrix} E_\theta^s \\ E_\phi^s \end{pmatrix} \tag{3}$$

#142019 - $15.00 USD Received 31 Jan 2011; revised 21 Mar 2011; accepted 21 Mar 2011; published 29 Mar 2011

This coordinate transformation depends only upon the azimuthal angle ϕ. The radial location of the collimated field components is related to the focal length of the objective, f_o, and the scattering angle, θ, simply by $r(x, y) = f_o \times \cos\theta$. Finally, a tube-lens algorithm performs the two-dimensional Fourier transform of the collimated fields, $E_x^c(r, \phi)$ and $E_y^c(r, \phi)$, and forms the image of the microsphere-nanosphere system in the image plane located at the focal distance, f_θ, of the lens by:

$$\begin{pmatrix} E_X^o \\ E_Y^o \end{pmatrix} = F.T. \begin{Bmatrix} E_x^c \\ E_y^c \end{Bmatrix} \tag{4}$$

Figure 4 illustrates an example of the accuracy of this tool in computationally synthesizing images of micron-scale objects. This figure compares the experimental and computed images of two adjacent, contacting, polystyrene microspheres (in air) of diameter 4.3 μm. An NA = 0.6 was used, assuming illumination wavelengths between 400 and 700 nm. Each image is normalized by its maximum intensity, and the same gray scale is used for both. We observe good agreement between the experimental and numerical images.

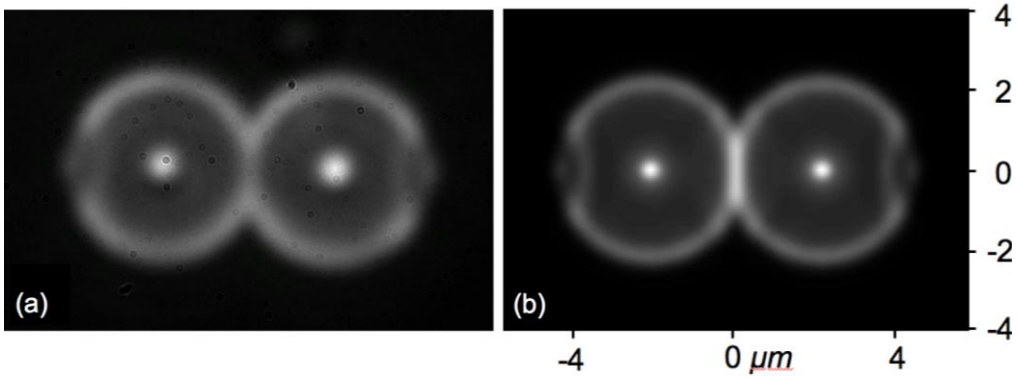

Fig. 4. Comparison of experimental (a) and computed (b) images of two 4.3 μm diameter polystyrene microspheres for NA = 0.6 and wavelengths between 400 nm and 700 nm.

5. Backscattering enhancement measurements

We now report measurements and comparative numerical results for the sample platform of Fig. 1 and the imaging system of Fig. 3. Here, a 4.4 μm diameter $BaTiO_3$ microsphere was embedded in solid PDMS, and a gold nanoparticle of diameter either 50 nm, 60 nm, 80 nm, or 100 nm was positioned in liquid PDMS 350 nm above the microsphere within its nanojet. An unpolarized broadband visible-light (λ_0 = 400 to 700 nm) plane wave illuminated the system, and the backscattered intensities were measured. Imaging results for this system are shown in Fig. 5.

Figure 5 qualitatively illustrates the visible-light backscattering enhancement caused by a 100 nm gold nanoparticle located within the nanojet of the 4.4 μm diameter $BaTiO_3$ microsphere embedded in PDMS. In Fig. 5, both images are normalized by the maximum intensity, 1669, of the central peak in Fig. 5(b), with the same gray scale used for both images and the background signal not removed. From Fig. 5(b), it is clear that the presence of the gold nanoparticle in the nanojet of the microsphere significantly enhanced the microsphere's visibility. Otherwise, when isolated, the microsphere was barely visible above the background, as shown in Fig. 5(a). (Note that Fig. 5(b) does not show the "rings" seen in Fig.

#142019 - $15.00 USD Received 31 Jan 2011; revised 21 Mar 2011; accepted 21 Mar 2011; published 29 Mar 2011

4 because: (a) the intensity of the rings is very small relative to the central peak generated by the nanoparticle; and (b) the sharpness of the rings is reduced by the comparatively low value of NA = 0.12 used to obtain Figs. 5(a) and 5(b) vs. NA = 0.6 used to obtain Fig. 4.)

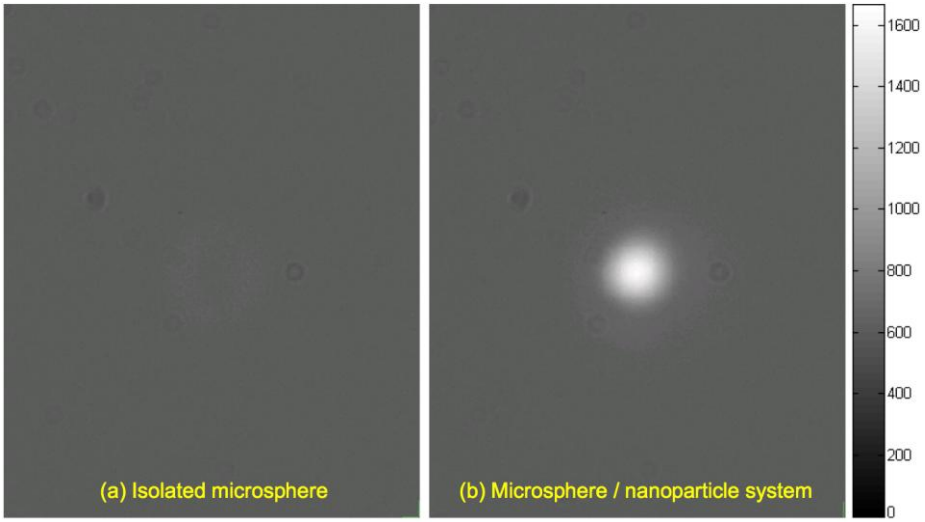

Fig. 5. Comparison of two experimental visible-light backscattering images: (a) isolated 4.4 μm diameter $BaTiO_3$ microsphere in PDMS; (b) microsphere of (a) with a 100 nm gold nanoparticle located 350 nm above the microsphere within its nanojet. 5X magnification and NA = 0.12.

Figure 6(a) shows computational modeling results for the normalized backscattering intensity enhancement as a function of the NA for the experiment of Fig. 5. These results reveal that the enhancement factor initially rises as the NA is increased from zero. The enhancement factor reaches a maximum value of about 65 when the NA is approximately 0.075, corresponding to a scattering integration angle between 175° and 180°. Thereafter, the enhancement factor decreases rapidly. Note that the previously reported dimensionally scaled microwave measurements of backscattering enhancement [10,11] used what amounted to be a zero-NA detection system.

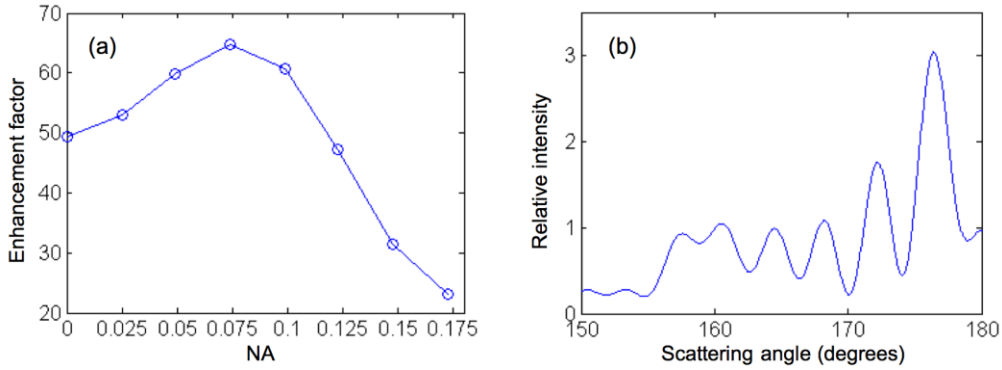

Fig. 6. (a) Computationally modeled NA dependence of the backscattering intensity enhancement caused by a 100-nm gold nanoparticle for the broadband illumination case of Fig. 5. (b) Typical monochromatic scattering intensity of the microsphere vs. scattering angle θ.

#142019 - $15.00 USD Received 31 Jan 2011; revised 21 Mar 2011; accepted 21 Mar 2011; published 29 Mar 2011

The reason why the maximum backscattering enhancement occurs for a nonzero NA can be deduced by considering Fig. 6(b), which plots a typical monochromatic, ϕ-symmetric, scattering intensity pattern of the microsphere/nanoparticle system vs. the scattering angle θ. Here, we see that the scattering intensity oscillates as θ decreases from 180° (direct backscattering). For a nonzero collection angle defined by the NA of the objective, fields scattered at smaller angles than 180° are summed coherently to form an image in the image plane. Due to the angular oscillation of the scattered field, the total intensity for a nonzero NA has a maximum value at θ corresponding to the first peak in Fig. 6(b).

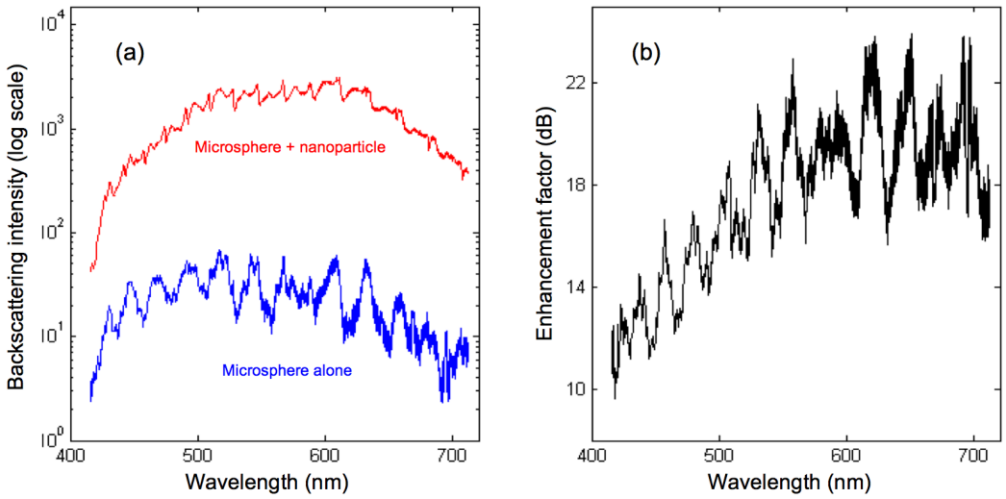

Fig. 7. (a) Measured backscattering spectral responses of the 4.4 μm diameter $BaTiO_3$ microsphere with and without the nearby perturbing 100 nm diameter gold nanoparticle for an objective NA = 0.12. (b) Spectral response of the backscattering enhancement based upon the data of (a).

Figure 7(a) depicts the measured backscattering spectral responses of the 4.4 μm diameter $BaTiO_3$ microsphere with and without the nearby perturbing 100 nm diameter gold nanoparticle for an imaging objective NA of 0.12. Figure 7(b) plots the spectral response of the backscattering intensity enhancements corresponding to the data of Fig. 7(a). We observe that the enhancement factor exhibits repetitive peaks similar to the numerical results shown in Fig. 2, although the heights of these peaks are smaller than the numerical ones. Background noise and the limited resolution of the spectrometer used in the measurements may have contributed to this difference. Despite this limitation, measured enhancement factors reached almost 24 dB at wavelengths between 600 and 700 nm. We note that these large enhancements reduce to about 17 dB when the spectral intensities are integrated.

Figure 8 depicts the dependence of the backscattering intensity enhancement upon the diameter of the gold nanoparticle in the nanojet. The upper blue dotted line with star marks shows the GMM-calculated backscattering intensities as a function of the gold nanoparticle size for free-space, λ_0 = 400 nm, plane-wave illumination of the 3.5 μm polystyrene microsphere / gold nanoparticle system reported in [8]. In [8], gold nanoparticles sized from 2 to 60 nm yielded the slope $m \cong 3.3$, whereas $m \cong 5.1$ was obtained for nanoparticles sized from 50 to 100 nm.

#142019 - $15.00 USD Received 31 Jan 2011; revised 21 Mar 2011; accepted 21 Mar 2011; published 29 Mar 2011

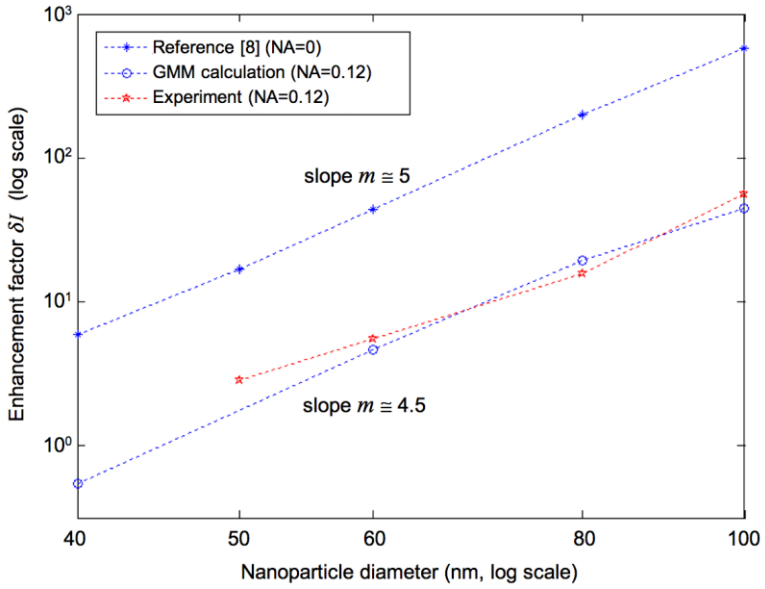

Fig. 8. Measured and modeled backscattering intensity enhancements as a function of the gold nanoparticle diameter.

The two lower curves in Fig. 8 are our experimental results (red dotted line with star marks) and our computational model results (blue dotted line with circle marks) for the backscattering enhancements obtained with the system of Figs. 1 and 3 for an objective NA of 0.12. The measured and modeled results agree well for gold nanoparticle sizes of 50, 60, 80, and 100 nm. Relative to the results in [8], our measured slope $m \cong 4.5$ is smaller, and the enhancement factor is reduced by 10 dB because of the averaging effect over the broadband illumination wavelengths that we used.

Despite our smaller measured backscattering enhancements relative to what Ref. [8]. obtained theoretically for monochromatic illumination, Fig. 8 shows that a gold nanoparticle as small as 50 nm can be readily detected using broadband visible light via the nanojet backscattering enhancement phenomenon. This size nanoparticle caused a measured 3:1 (200%) increase in the measured backscattering intensity of the adjacent 4.4 μm diameter microsphere when positioned within its nanojet.

6. Summary and conclusions

In this paper, we reported what we believe is the first experimental confirmation at visible light wavelengths of the backscattering enhancement phenomenon of the photonic nanojet emitted by a dielectric microsphere. A specially designed sample stage consisting of a multilayered sandwich of glass, solid PDMS, and liquid PDMS, permitted the precise positioning of a gold nanoparticle of diameter between 50 and 100 nm within the nanojet emitted by a 4.4 μm diameter $BaTiO_3$ microsphere. A conventional microscope imaging system with a low numerical aperture (NA) objective was used to generate a backscattered image of the microsphere/nanoparticle system using broadband visible light as the illumination. We also formulated a numerical model incorporating Mie-based theory and Fourier optics which agreed well with the measurements.

Via measurements and computational modeling, we determined that the backscattering enhancement is strongly dependent upon the illumination wavelength and NA of the imaging system. The largest backscattering enhancements occur for nonresonant illuminations of the

#142019 - $15.00 USD Received 31 Jan 2011; revised 21 Mar 2011; accepted 21 Mar 2011; published 29 Mar 2011

microsphere (when considered in isolation). Low objective NAs of approximately 0.075 yield the maximum observed increases in backscattering. Due to the wavelength-averaging scheme of the broadband imaging system, the measured peak backscattering enhancement was found to be about 10 dB less than calculated theoretically for monochromatic illumination.

We demonstrated experimentally that a gold nanoparticle as small as 50 nm can be readily detected using broadband visible light via the nanojet backscattering enhancement phenomenon. This size nanoparticle caused a measured 3:1 (200%) increase in the measured backscattering intensity of the adjacent 4.4 μm diameter microsphere when positioned within its nanojet. We found that this backscattering enhancement factor can be further increased if the objective NA is adjusted to the optimum value.

Overall, the backscattering enhancement phenomenon of the photonic nanojet affords the possibility of broadband visible light detection of gold nanoparticles even smaller than 50 nm. The lower bound on the detectable nanoparticle size will ultimately be determined by the dynamic range of the optical measurement system, i.e., its ability to distinguish fractional (less than 100%) enhancements of the backscattering of the nanojet-generating microsphere in the presence of the background.

Acknowledgments

This work was supported by National Institutes of Health (NIH) grant R01 EB003682 and National Science Foundation (NSF) grant CBET-0937987. Dr. Kwonnam Sohn of Prof. Jiaxing Huang's research group in Northwestern's Materials Science and Engineering Department provided the 100 nm gold nanoparticles used in this research.

#142019 - $15.00 USD Received 31 Jan 2011; revised 21 Mar 2011; accepted 21 Mar 2011; published 29 Mar 2011